Hindawi
Mathematical Problems in Engineering
Volume 2019, Article ID 8279435, 11 pages
https://doi.org/10.1155/2019/8279435

Research Article

Full-Life-Cycle Analysis of Cement Sheath Integrity

Jie Hu,[1,2] **Linlin Wang**,[3] **Jili Feng**,[1] **Jiyun Shen**,[4] **and Manchao He**[1]

[1]*State Key Laboratory for Geomechanics and Deep Underground Engineering, China University of Mining and Technology, Beijing 100083, China*
[2]*School of Mechanics and Civil Engineering, China University of Mining and Technology, Beijing 100083, China*
[3]*College of Petroleum Engineering, China University of Petroleum, Beijing 102249, China*
[4]*Drilling Research Institute, CNPC, Beijing 102206, China*

Correspondence should be addressed to Linlin Wang; linlin.wang@cup.edu.cn

Received 7 June 2019; Revised 16 September 2019; Accepted 16 November 2019; Published 28 December 2019

Academic Editor: Rafael Morales

This paper addresses evaluating the evolution of stress inside the casing-cement sheath-formation system during the cement injection, setting, completion, and production stages of hydrocarbon recovery. This full-life-cycle analysis of cement sheath integrity gives rise to assessment of potential failure mode (i.e., tensile mode, shear mode, and microannulus) in different stages, and the prevention measures can be proposed accordingly. Considering the loading history, two regimes should be distinguished. Before the accomplishment of cementation, as the cement slurry can merely withstand its hydraulic pressure, the in situ stress and the wellbore pressure are withstood by the rock and the casing, respectively. Once the cementation process is completed, the stress increment (e.g., hydraulic fracturing pressure) is withstood by the casing-cement sheath-formation system. The autogenous shrinkage of cement adversely affects the resistance of the system to all types of failure, whereas a moderate swelling of cement is favorable to the cement sheath integrity. In addition, the cement sheath integrity is strongly influenced by the depth: the failure is encountered more easily at the shallow layer. Both the hydraulic fracturing pressure in the completion stage and the increase in casing temperature in the production stage may lead to tensile circumferential stress, and the hydraulic fracturing is the most critical stage for the integrity of cement sheath.

1. Introduction

Maintaining well integrity in the whole life of hydrocarbon recovery is a key issue adversely impacting the effective and economic production [1–3]. This issue becomes more severe when exploiting deep resources in recent decades. High temperature and high pressure (HTHP) have to be dealt with at increasing depths, and more rigorous design is required to ensure the well integrity [4]. In addition, hydraulic fracturing has been employed more and more extensively for unconventional resources such as shale gas. The high casing pressure encountered in hydraulic fracturing tremendously challenges the well integrity [5–7].

The sealing failure could be in different types including shear or tensile failure of cement sheath [8] and microannulus at the cement-casing interface (first interface) or cement-formation interface (second interface) [9–11]. If the potential failure mode is correctly estimated, measures can be accordingly taken to ensure the well integrity. For instance, high-strength cement could be used to prevent tensile and shear failure of cement sheath. To avoid the risk of microannulus, cementing technologies that strengthen contact force of cement sheath with casing and formation can be taken such as using the expansive cement slurry system, applying annular pressure during cement setting, and reducing fluid density during cement setting. The loss of well integrity is strongly governed by the stress.

After drilling, a well sequentially experiences cement injection, cement setting, completion, and production stages. Main mechanisms causing the failure of well integrity in these stages include the shrinkage of cement

sheath due to cement hydration [9], the increase in internal casing pressure during hydraulic fracturing [7], and the increase in casing temperature when producing deep oil/gas [4]. These factors have been extensively investigated [11, 12]. A novel cement sheath mechanical model has been introduced to reflect the failure modes of radial cracking, shear failure, and microannulus considering thermal loads, wellbores fracture, and coupling loads [13, 14]. The finite element method was useful to evaluate wellbore and near-wellbore stresses during fracture creation and propagation [15]. However, most of these studies focused on analysis of stress under single operating condition, but the influence of the stress state in the previous stage to the subsequent stage has been rarely discussed. Only a few scholars considered the entire cement injection, cement setting, completion, and production stages. The comprehensive analytical and numerical models for stress distributions around an inclined, cased wellbore by considering all wellbore processes are developed to apply to cement sheath failure [16]. Second, most studies applied formation stress directly to the casing-cement-formation system [12], which may lead to an incorrect estimation of the true stress state of the system. Actually, during cement injection, the cement slurry is in liquid form, which can merely understand hydraulic pressure rather than the anisotropic in situ stress in the formation. Third, conventional cement shrinks during hydration [9, 17], which may result in redistribution of stress. However, this factor has not been systematically investigated in the risk assessment of well integrity.

In the full life cycle of a well, the stress state changes in all stages, and the stress state of the former stage will have an impact on the subsequent stage. Therefore, a thorough analysis of the evolution of stress in various stages of the full life cycle is required. In this context, a full-life-cycle analysis of the stress evolution inside the casing-cement-formation system is conducted in this work. Possible failure mode of cement sheath integrity at each state is analyzed accordingly, providing reference to take effective measures for maintaining well integrity.

2. Mathematical Modeling

Analysis in this study is based on a deep well (vertical depth 6300 m) in Tarim oilfield, China. The fluid density in the casing $s\rho_w = 1.0\,\text{g/cm}^3$, and the density of cement slurry $\rho_c = 1.9\,\text{g/cm}^3$. As the difference between the maximum and minimum horizontal in situ stress is very small (at the depth of 6300 m, $\sigma_H = 140\,\text{MPa}$ and $\sigma_h = 134\,\text{MPa}$), the minimum and maximum in situ stress of the well is considered equal, with an equivalent density of $2.0\,\text{g/cm}^3$.

Schematics of the casing-cement sheath-formation (CSF) system are shown in Figure 1, where r_1, r_2, and r_3 represent casing inner radius, casing outer radius, and cement sheath outer radius, respectively. The elastic properties of the casing, cement, and rock are listed in Table 1. Considering the geometry of the system, the cylindrical coordinate system (r, θ, z) is used. The problem is plane strain because the axial dimension of the well is much larger than the in-plane dimensions. Further assumptions are proposed: (1) the casing, cement, and rock are all isotropic elastic; (2) the casing and cement sheath are ideally cylindrical; (3) the casing is completely centered, and the cement sheath completely fills the annulus space; and (4) the effect of outer technology casing is ignored. In this work, tensile stress is considered positive, and compressive stress is considered negative. The evolution of stress of the system for four stages is investigated: cement injection, cement setting, well completion, and production.

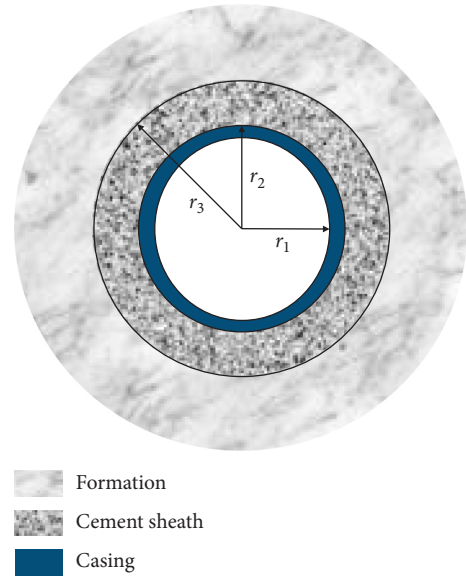

Figure 1: Schematics of the casing-cement sheath-formation system.

It should be noted that the cement and rock are porous media, and their mechanical responses are also governed by the pressure of fluid within the pores [18–20]. However, the casing and cement are impermeable and low permeable so that the variation of pore pressure in the CSF system is relatively slow [21]. In comparison, the failure commonly occurs at the immediateness of varying boundary conditions. Therefore, the poromechanical behaviors are not considered in the present work.

3. Cement Injection Stage

In the cement injection stage, the cement slurry is in liquid phase and can merely withstand hydraulic pressure, so the stress state of cement slurry is $\sigma_{rr} = \sigma_{\theta\theta} = -P_c = -\rho_c g h$, where ρ_c is the density of cement slurry and h is the depth. With regards to the formation (i.e., rock), it is subjected to in situ stresses (the maximum and minimum horizontal stresses σ_H and σ_h) at the outer boundary and hydrostatic pressure of the cement slurry $(-P_c)$ at the inner boundary. This is a typical Kirsch problem [22], for which the solution is as follows:

Table 1: The geometrical and mechanical properties of the CSF system.

	Inner radius (mm)	Outer radius (mm)	Young's modulus (GPa)	Poisson's ratio	Thermal conductivity (W/m·K)	Coefficient of thermal expansion (10^{-6}(°C))
Casing	85.725	98.425	210	0.25	50	11.59
Cement sheath	98.425	122.685	10	0.20	0.58	10.0
Formation	122.685	∞	60	0.18	2	7

$$\begin{cases} \sigma_{rr}^{\mathrm{r}} = -\dfrac{\sigma_{\mathrm{H}}+\sigma_{\mathrm{h}}}{2}\left(1-\dfrac{r_3^2}{r^2}\right)-\dfrac{\sigma_{\mathrm{H}}-\sigma_{\mathrm{h}}}{2}\left(1+3\dfrac{r_3^4}{r^4}-4\dfrac{r_3^2}{r^2}\right)\cos 2\theta-\dfrac{P_{\mathrm{c}}r_3^2}{r^2}, \\ \sigma_{\theta\theta}^{\mathrm{r}} = -\dfrac{\sigma_{\mathrm{H}}+\sigma_{\mathrm{h}}}{2}\left(1+\dfrac{r_3^2}{r^2}\right)+\dfrac{\sigma_{\mathrm{H}}-\sigma_{\mathrm{h}}}{2}\left(1+3\dfrac{r_3^4}{r^4}\right)\cos 2\theta+\dfrac{P_{\mathrm{c}}r_3^2}{r^2}, \\ \sigma_{r\theta}^{\mathrm{r}} = \dfrac{\sigma_{\mathrm{H}}-\sigma_{\mathrm{h}}}{2}\left(1-3\dfrac{r_3^4}{r^4}+2\dfrac{r_3^2}{r^2}\right)\sin 2\theta, \end{cases} \tag{1}$$

where θ is the angle from the maximum horizontal stress σ_{H}.

The casing undergoes the fluid column pressure ($P_{\mathrm{w}} = -\rho_{\mathrm{w}}gh$) at the inner boundary and $-P_{\mathrm{c}}$ at the outer boundary. This is a classical Lamé problem, and the analytic solution is as follows:

$$\begin{cases} \sigma_{rr}^{\mathrm{w}} = \dfrac{P_{\mathrm{c}}r_2^2-P_{\mathrm{w}}r_1^2}{r_1^2-r_2^2}-\dfrac{(P_{\mathrm{c}}-P_{\mathrm{w}})r_1^2r_2^2}{(r_1^2-r_2^2)r^2}, \\ \sigma_{\theta\theta}^{\mathrm{w}} = \dfrac{P_{\mathrm{c}}r_2^2-P_{\mathrm{w}}r_1^2}{r_1^2-r_2^2}+\dfrac{(P_{\mathrm{c}}-P_{\mathrm{w}})r_1^2r_2^2}{(r_1^2-r_2^2)r^2}, \\ \sigma_{r\theta}^{\mathrm{w}} = 0. \end{cases} \tag{2}$$

The stress state of the CSF system at the depth of 6300 m is shown in Figure 2. In this stage, the casing, cement sheath, and formation undertake compressive stress, among which the maximum is the tangential stress within the casing mainly due to the high stiffness of the casing. Figure 3 shows the stress state of the CSF system if the equivalent density of in situ stress is taken as 1.5 g/cm^3. Comparing Figures 2 and 3, we can find that with different in situ stress, only the stress state of the formation is different, while the stress state of the cement and casing is the same. This result can be explained as follows: due to extraction of the rock initially occupying the borehole during drilling, the pressure applied at the borehole changes from the initial in situ stress to the hydraulic pressure of drilling fluid. In the cement injection stage, the cement slurry is in liquid state, and it only undertakes the hydrostatic pressure of its own. Hence, the pressure change at the borehole is balanced by the deformation of the rock, whereas the initial in situ stress cannot transfer to the cement slurry and the casing. Similarly, the fluid pressure within the casing is only taken by the casing and cannot transfer to the cement slurry and formation.

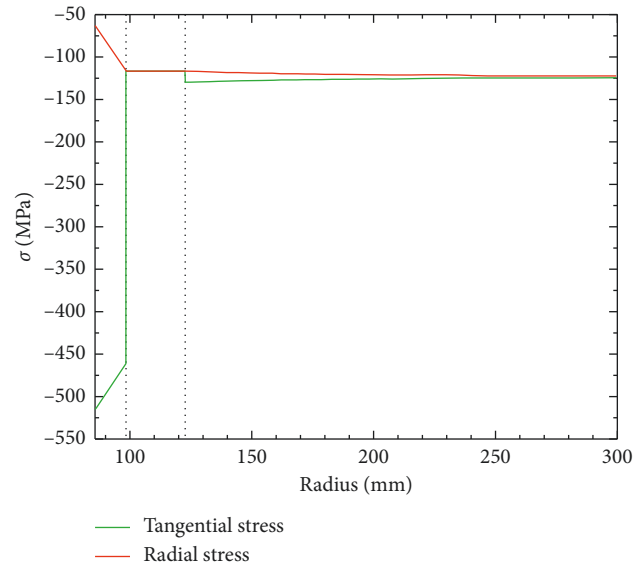

Figure 2: The stress state of the CSF system in the cement injection stage at 6300 m (in situ stress equivalent density of 2 g/cm^3).

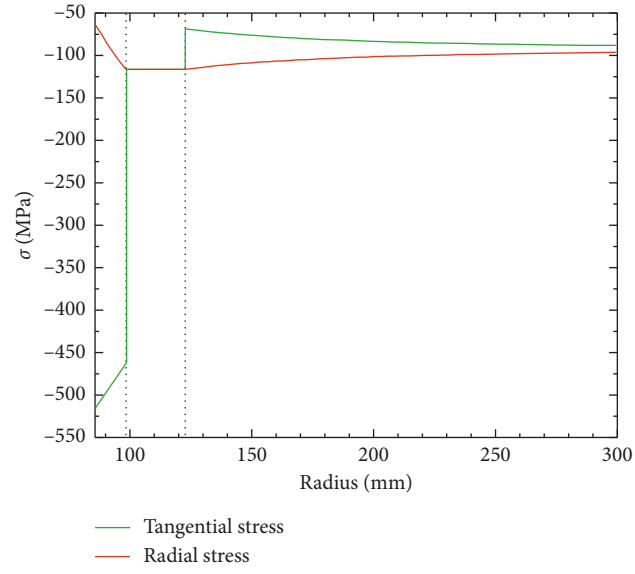

Figure 3: The stress state of the CSF system in the cement injection stage at 6300 m (in situ stress equivalent density of 1.5 g/cm^3).

4. Cement Setting Stage

Once the cement is injected, the cement slurry gradually changes from liquid state to solid state due to hydration;

thus, the cement will be considered as solid from now on [23]. The volume of cement sheath will shrink or expand according to the formula of cement slurry during the hydration. The volume change of cement sheath can be considered as free strain ε^{c}, namely, strain generated without stress. The focus of this paper is to evaluate the evolution of the stress inside the casing-cement-formation system during the different stages of hydrocarbon exploitation. In particular, the cement injection and setting stages are considered here, and we reveal that the stress evolution when considering the two stages is totally different from the existing analysis that commonly neglect them [12]. This is the main originality of this paper. To highlight the comparison with the existing model, we prefer to obtain close-form solutions of the stress evolution. The analytical solution cannot be obtained when considering the plasticity. With this purpose, we assume the cement as an ideal elastic material.

Due to the axis symmetry of the CSF system and the isotropy of free strain and of elastic material, only radial displacement u takes place, and the increment of stress and strain in this stage is only related with r. Basic equations of plane axisymmetric problem in cylindrical system are as follows:

Equilibrium equation:

$$\frac{\partial \sigma_{rr}}{\partial r} + \frac{\sigma_{rr} - \sigma_{\theta\theta}}{r} = 0. \tag{3}$$

Compatibility relationship:

$$\begin{aligned} \varepsilon_{rr} &= \frac{\mathrm{d}u}{\mathrm{d}r}, \\ \varepsilon_{\theta\theta} &= \frac{u}{r}. \end{aligned} \tag{4}$$

Constitutive equations:

$$\begin{cases} \varepsilon_{rr} = \dfrac{\sigma_{rr}}{E^{\mathrm{i}}} - \dfrac{\nu^{\mathrm{i}}}{E^{\mathrm{i}}}\left(\sigma_{\theta\theta} + \sigma_{zz}\right) + \varepsilon^{\mathrm{i}}, \\ \varepsilon_{\theta\theta} = \dfrac{\sigma_{\theta\theta}}{E^{\mathrm{i}}} - \dfrac{\nu^{\mathrm{i}}}{E^{\mathrm{i}}}\left(\sigma_{rr} + \sigma_{zz}\right) + \varepsilon^{\mathrm{i}}, \\ \varepsilon_{zz} = \dfrac{\sigma_{zz}}{E^{\mathrm{i}}} - \dfrac{\nu^{\mathrm{i}}}{E^{\mathrm{i}}}\left(\sigma_{\theta\theta} + \sigma_{rr}\right) + \varepsilon^{\mathrm{i}}. \end{cases} \tag{5}$$

Equation (5) is similar to the thermoelasticity problem, in which the total strain consists of two parts: the elastic strain (obeys Hooke's law) and the free strain. In this work, the most general situation is considered, where free strain can take place in the casing, cement sheath, or formation. The superscript i can represent casing (w), cement sheath (c), and rock (r). In the cement setting stage, we have $\varepsilon^{c} \neq 0$, while $\varepsilon^{w} = \varepsilon^{r} = 0$.

Substituting equations (4) and (5) into equation (3), we get the general equation in terms of u:

$$\frac{\partial^2 u}{\partial r^2} + \frac{1}{r}\frac{\partial u}{\partial r} - \frac{u}{r^2} = 0. \tag{6}$$

Basic solution of this differential equation is

$$u^{\mathrm{i}} = X^{\mathrm{i}} r + \frac{Y^{\mathrm{i}}}{r}, \tag{7}$$

where X^{i} and Y^{i} are two constants that can be determined by boundary conditions. Substituting equations (4) and (7) into equation (5) yields the expression of stress component:

$$\begin{cases} \sigma_{rr} = \dfrac{E^{\mathrm{i}}}{1+\nu^{\mathrm{i}}}\left(X^{\mathrm{i}} - \dfrac{Y^{\mathrm{i}}}{r^2}\right) + 2X^{\mathrm{i}}\dfrac{E^{\mathrm{i}}\nu^{\mathrm{i}}}{(1+\nu^{\mathrm{i}})(1-2\nu^{\mathrm{i}})} + \dfrac{E^{\mathrm{i}}\varepsilon^{\mathrm{i}}}{2\nu^{\mathrm{i}}-1}, \\ \sigma_{\theta\theta} = \dfrac{E^{\mathrm{i}}}{1+\nu^{\mathrm{i}}}\left(X^{\mathrm{i}} + \dfrac{Y^{\mathrm{i}}}{r^2}\right) + 2X^{\mathrm{i}}\dfrac{E^{\mathrm{i}}\nu^{\mathrm{i}}}{(1+\nu^{\mathrm{i}})(1-2\nu^{\mathrm{i}})} + \dfrac{E^{\mathrm{i}}\varepsilon^{\mathrm{i}}}{2\nu^{\mathrm{i}}-1}, \\ \sigma_{zz} = 2X^{\mathrm{i}}\dfrac{E^{\mathrm{i}}\nu^{\mathrm{i}}}{(1+\nu^{\mathrm{i}})(1-2\nu^{\mathrm{i}})} + \dfrac{E^{\mathrm{i}}\varepsilon^{\mathrm{i}}}{2\nu^{\mathrm{i}}-1}. \end{cases} \tag{8}$$

Equation (8) holds in the casing, cement sheath, and formation. Each part contains two unknown parameters (X^{i} and Y^{i}), so there are totally six unknowns to be determined by boundary conditions. In the cement setting stage, compared with the cement injection stage, the pressure in casing does not change, nor does the in situ stress applied at the outer boundary of the formation. Meanwhile, it is assumed that the casing, cement sheath, and rock are in perfect contact, so the boundary conditions are as follows:

Stress boundary conditions:

$$\begin{cases} \left(\sigma_{rr}^{\mathrm{w}}\right)_{r=r_1} = 0, \\ \left(\sigma_{rr}^{\mathrm{w}}\right)_{r=r_2} = \left(\sigma_{rr}^{\mathrm{c}}\right)_{r=r_2}, \\ \left(\sigma_{rr}^{\mathrm{c}}\right)_{r=r_3} = \left(\sigma_{rr}^{\mathrm{r}}\right)_{r=r_3}, \\ \left(\sigma_{rr}^{\mathrm{r}}\right)_{r\longrightarrow\infty} = 0. \end{cases} \tag{9}$$

Displacement boundary conditions:

$$\begin{cases} \left(u^{\mathrm{w}}\right)_{r=r_2} = \left(u^{\mathrm{c}}\right)_{r=r_2}, \\ \left(u^{\mathrm{c}}\right)_{r=r_3} = \left(u^{\mathrm{r}}\right)_{r=r_3}. \end{cases} \tag{10}$$

The six unknowns (X^{w}, Y^{w}, X^{c}, Y^{c}, X^{r}, Y^{r}) can be solved from boundary condition equations (9) and (10) so that the stress state of the CSF system in the cement setting stage is obtained.

Considering the free strain of cement sheath 0, 0.2% (expansion), and −0.2% (shrinkage), respectively, the radial and tangential stress caused by free strain is as shown in Figure 4.

In this stage, as liquid pressure in the casing and in situ stress does not change, no stress change occurs in the system if the volume change of the cement is null. When the volume of cement changes, the free strain of cement is restricted by the casing and formation, and additional stress is generated.

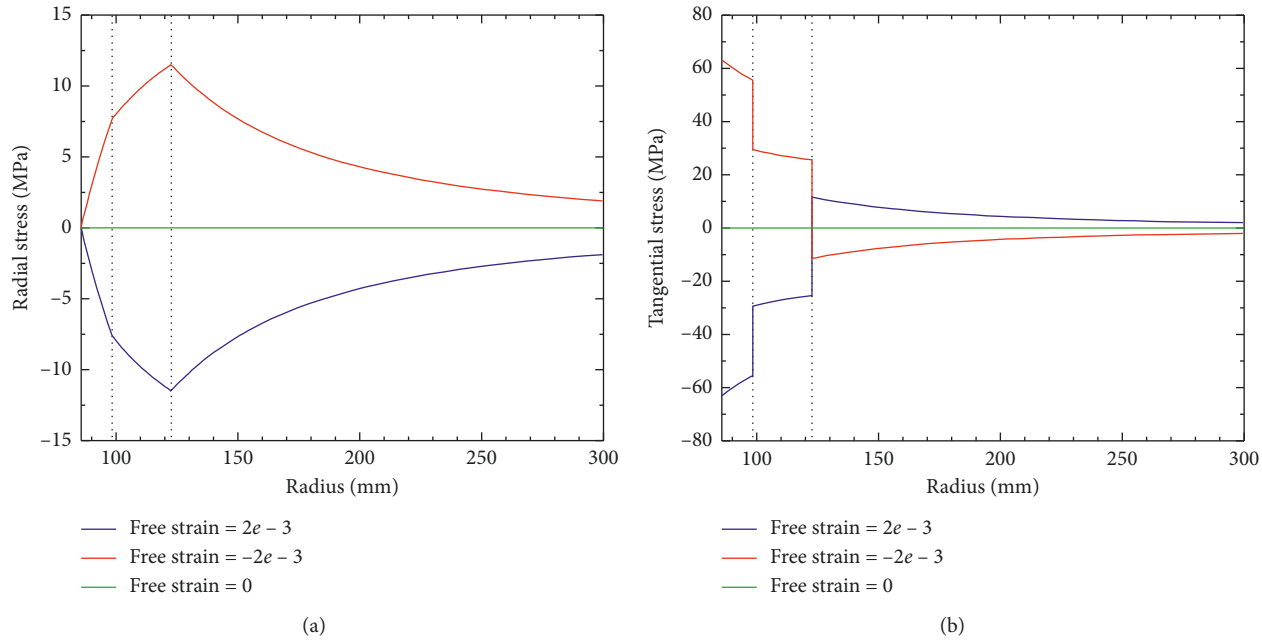

Figure 4: Stress caused by free strain of cement sheath.

When the free strain of cement is −0.2%, radial tensile stress is generated in the CSF system, and the maximum takes place at the second interface. The tangential stress is tensile in the casing and cement sheath and changes to be compressive in the formation. For the cement sheath, the maximum radial tensile stress locates at the second interface (11.5 MPa), and the maximum tangential tensile stress appears at the first interface (29.4 MPa). When the free strain of cement sheath is 0.2%, the stress sign (tensile or compressive) changes, and the absolute value remains the same as the case of −0.2%.

Figure 4 illustrates the stress increment during the cement setting stage, and the actual stress should be the sum of the stress state in the cement injection stage and the stress increment in the cement setting stage. As this work focuses on the cement sheath integrity, in the following, only the stress distribution of the cement sheath is presented. Figure 5 illustrates the actual stress state of the cement sheath at the end of the cement setting stage considering different volume changes of cement.

From Figure 5, we can find that although cement shrinkage produces radial tensile stress in the cement sheath, the total radial stress of cement sheath is still compressive when adding the stress state of the cement injection stage. When the shrinkage of cement increases, the radial compressive stress decreases, implying the contact stresses at the first and second interfaces decrease. In the following completion and production stage, if contact stress further decreases, the appearance of microannulus might occur. The tangential compressive stress of cement sheath also decreases when the cement shrinkage increases. When the free strain attains −0.1%, the tangential will be tensile, and tensile failure of the cement sheath would be triggered. It can also be found from Figure 5 that when cement sheath expands, the radial and tangential stresses become more compressive; thus, the capacity of the cement sheath to resist microannulus and tensile failure increases.

Besides the microannulus and the tensile failure, the cement sheath integrity may be degraded also by shear failure [24, 25]. The Mohr–Coulomb criterion is chosen as the criterion of the shear failure in the cement sheath, which has the following form:

$$F = \frac{1}{2} A \left(\sigma_{\theta\theta} - \sigma_{rr}\right) + \frac{1}{2} \left(\sigma_{\theta\theta} + \sigma_{rr}\right) \sin \varphi - C \cos \varphi. \quad (11)$$

In equation (11), parameter A is used to distinguish the maximum and minimum principal stress; $A = 1$ when $\sigma_{\theta\theta} > \sigma_{rr}$, while $A = -1$ for $\sigma_{\theta\theta} < \sigma_{rr}$. When the failure coefficient F is positive, shear failure occurs. We take the internal friction angle as 30° and the cohesive force as 11.5 MPa (corresponding to uniaxial compressive strength of 40 MPa); the value of F is given in Figure 6. It can be found that when the shrinkage of cement sheath increases, the failure coefficient F increases, namely, the cement sheath has the tendency of shear failure. When cement sheath expands, F does not change so much.

Figure 7 shows the stress at the inner surface of cement sheath at different depths. At the shallow section, the shrinkage of cement sheath will generate tensile stress; thus, microannulus and the tensile failure of cement sheath occur. This is mainly because at shallow depth, the hydrostatic pressure that the cement sheath undertakes during the cement injection stage is small compared to the tensile stress caused by cement shrinkage at the cement setting stage, so the total stress is tensile. With increasing depth, the compressive stress increases and the ability of cement sheath to resist the microannulus and tensile failure increases. Figure 8 presents the shear failure coefficient at the inner interface of

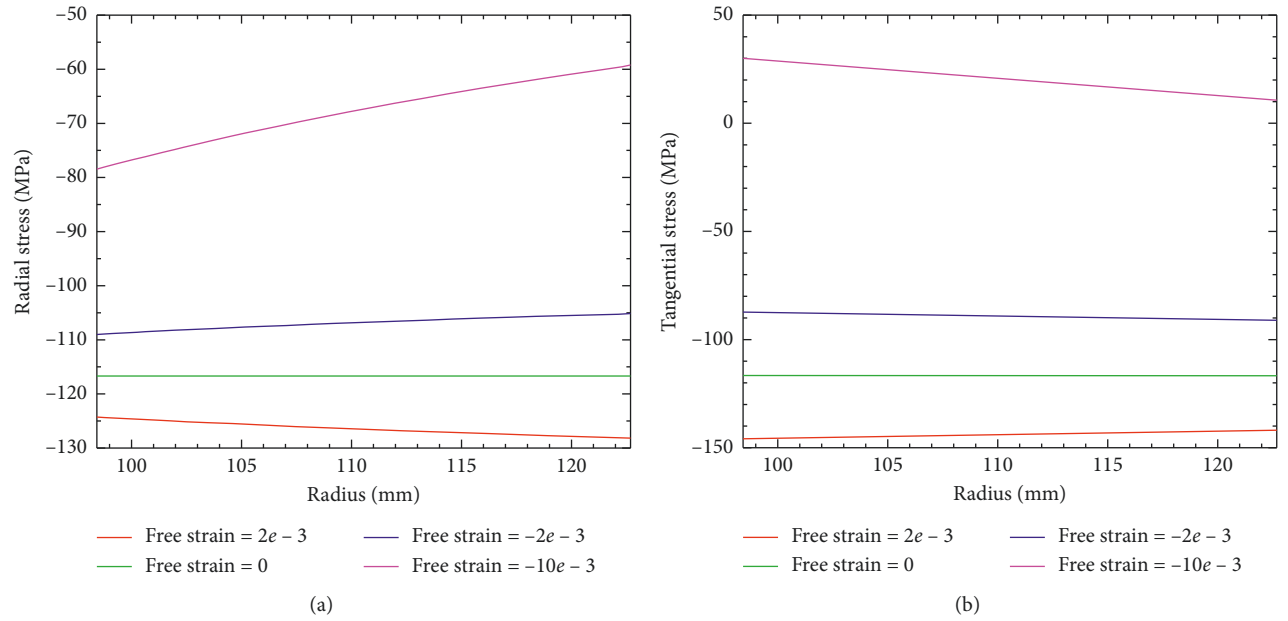

Figure 5: Total stress within the cement sheath in the cement setting stage at 6300 m.

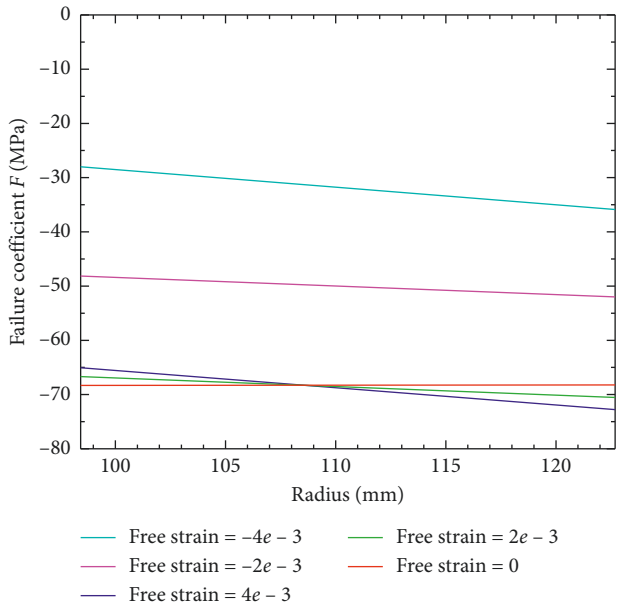

Figure 6: Failure coefficient of Mohr–Coulomb criterion in the cement setting stage at 6300 m.

cement sheath at different depths. It can be found that the greater the depth is, the smaller the F value is; thus, the ability of the cement sheath to resist shear failure increases.

From the above analysis, the cement volume change in the cement setting stage causes incremental stress within the CSF system, which affects the sealing ability of the system. When the cement sheath shrinks, the ability to resist tensile and shear failures and microannulus decreases; when cement sheath expends, the ability to resist tensile failure and microannulus increases, while the ability to resist shear failure changes slightly. Meanwhile, with increasing depth, the increase in the hydraulic pressure at the cement setting stage strengthens the cement sheath from all failure modes (tensile, shear failure, and microannulus).

5. Completion Stage

Hydraulic fracturing is commonly encountered in the completion stage, resulting in a change of casing pressure, i.e., $\Delta P_w = (\rho_f - \rho_w)gh + P_0$, where ρ_f is fracturing fluid density and P_0 is fracturing pressure applied at wellhead. Because the symmetry of the system remains, the stress increment of casing, cement sheath, and formation is the same as equation (8) (with the free strain εi being null). The boundary conditions are also similar to equation (9) (except the casing pressure varies) and equation (10).

Assuming $P_0 = 100$ MPa and $\rho_f = 1.1$ g/cm^3, the stress variation caused by the internal casing pressure change in this stage is as shown in Figure 9. Due to the increment of internal casing pressure, radial compressive stress is generated in the CSF system. In the tangential direction, tensile stress is generated in the casing and formation; inside the cement sheath, tensile stress is found at internal surface and compressive stress is found at external surface.

The total stress in this stage is the sum of initial stress and the stress increment of the current stage. The stress evolution with depth at the inner surface of cement sheath is shown in Figure 10. It can be seen that due to the effect of high pressure in casing, the radial compressive stress increases, and thus the risk of microannulus reduces. However, the tangential tensile stress increases, so the risk of tensile failure increases.

The evolution of the failure coefficient F with depth at the inner surface is shown in Figure 11. In comparison with the cement setting stage, F value increases in the completion stage, and thus the risk of shear failure increases. For the expanding cement sheath, the coefficient F slightly reduces.

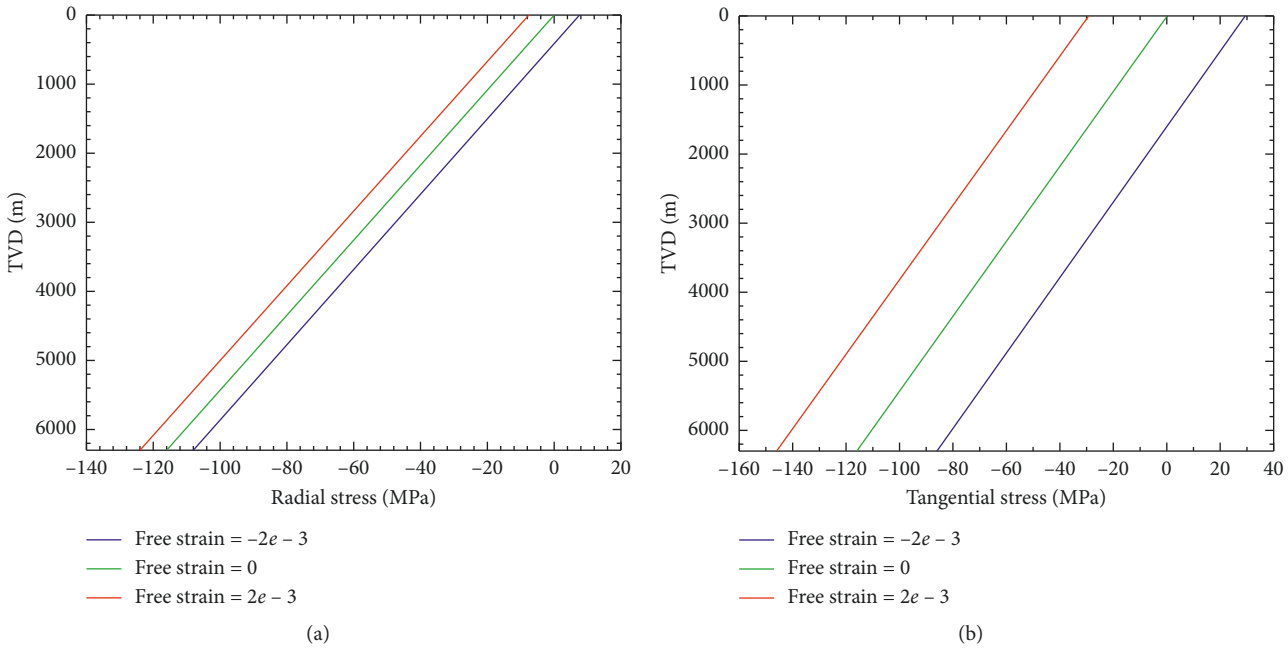

Figure 7: Stress at the inner surface of cement sheath at different depths in the cement setting stage.

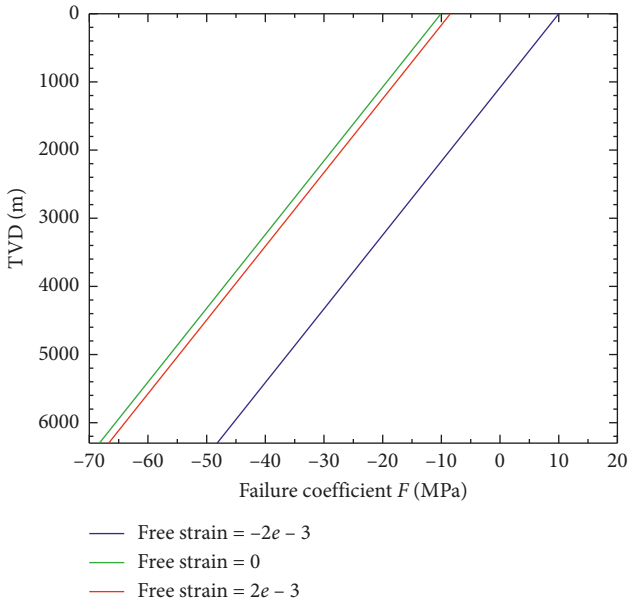

Figure 8: Failure coefficient at the inner surface of cement sheath at different depths in the cement setting stage.

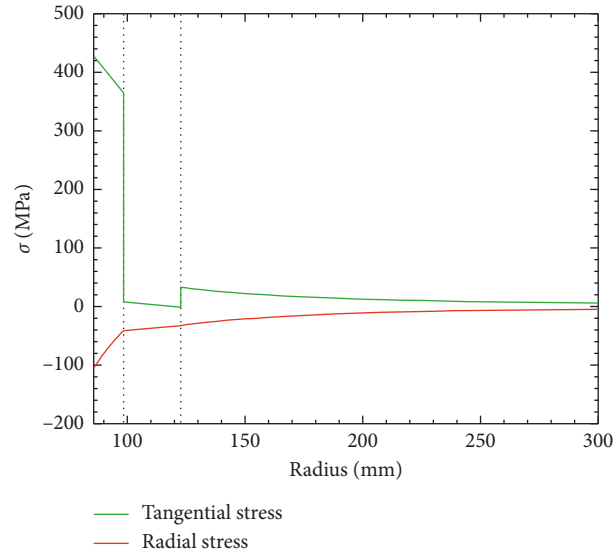

Figure 9: Stress change of the CSF system in the completion stage at 6300 m.

From Figures 10 and 11, tensile and shear failures and microannulus are all more prone in shallow section. The shrinkage of cement sheath has adverse effect on the system to resist all failure modes, whereas a moderate volume expansion of cement sheath (e.g., free strain = 0.2% in this work) is favorable for the cement sheath integrity.

When hydraulic fracturing is completed, the increase in wellhead pressure (100 MPa) disappears. Therefore, when calculating stress state in the subsequent stage, stress change at this stage should not be considered. It is worth noting that plastic deformation could take place in cement sheath during the process of fracturing, and when fracturing pressure unloads, there is a risk of microannulus in the system. The accumulation of plastic deformation may affect the integrity in the subsequent stage. Nevertheless, this paper does not consider the plasticity of the cement sheath, and a detailed study of the plastic behavior of cement sheath can be found in Chu et al. [11].

When calculating the stress stage in the completion stage, in situ stress and internal casing pressure are routinely applied directly to the CSF system. However, because of the cement being in liquid state during the cement injection

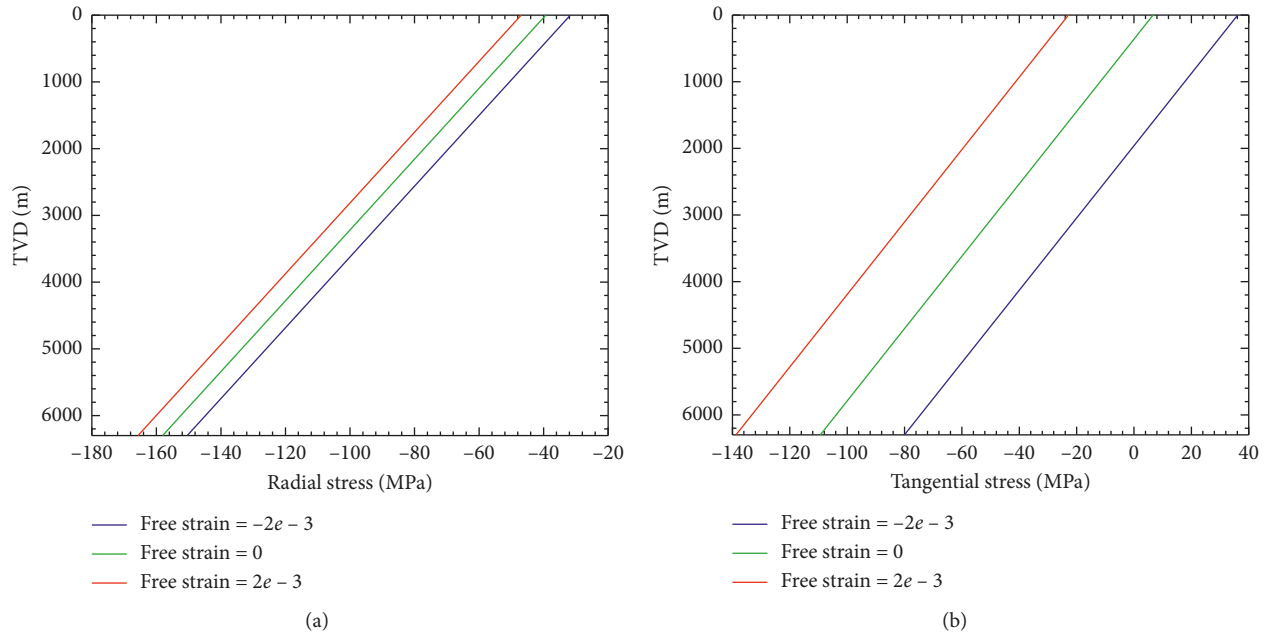

Figure 10: Stress at the inner surface of cement sheath at different depths in the completion stage.

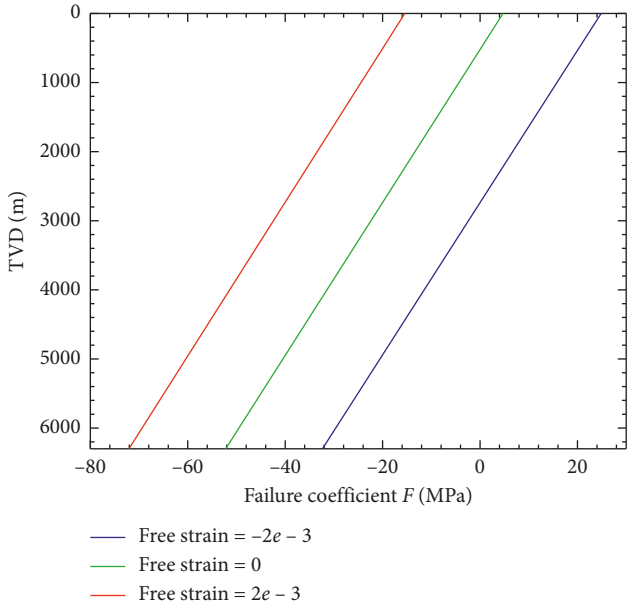

Figure 11: Failure coefficient at the inner surface of cement sheath at different depths in the completion stage.

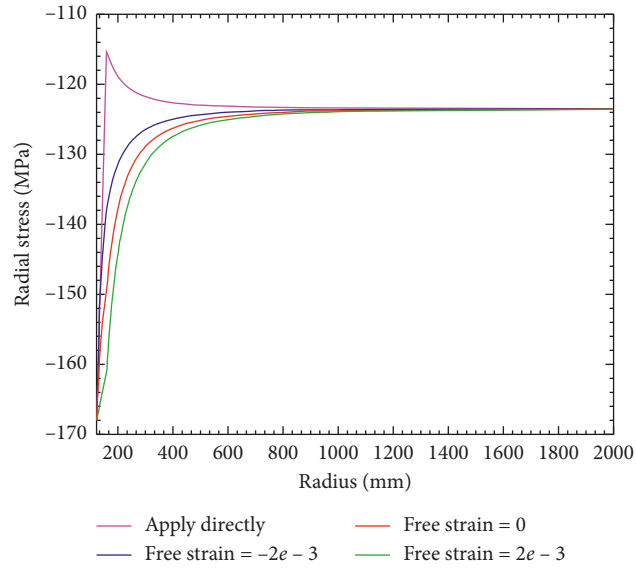

Figure 12: Stress state in the completion stage by different calculation methods at 6300 m.

stage, the in situ stress and fluid pressure in casing is actually undertaken by formation and casing, respectively, and only the stress variation (such as fracturing pressure) after cement setting could be applied to the whole CSF system. Hence, the routine method gives rise to an overestimation of the risk of the cement sheath integrity, as shown in Figure 12.

6. Production Stage

In the production stage, particularly for deep well, oil, and gas, with high temperature coming from the formation heat of the casing. Similar to the cement setting stage, the expansion of the casing due to heating leads to thermal stress. As discussed previously, this problem can also be treated as free-straining problem, and thus in equation (5), $\varepsilon^c = \alpha^i \Delta T$, where α^i is the coefficient of thermal expansion and ΔT is the temperature variation.

Assuming at certain depth, temperature at the inner surface of the casing increases 50°C, the stress variation is as shown in Figure 13. Radial compressive stress is generated in the CSF system, and the maximum radial stress appears at the first interface (about 11 MPa). The tangential stress in the casing is compressive, which has

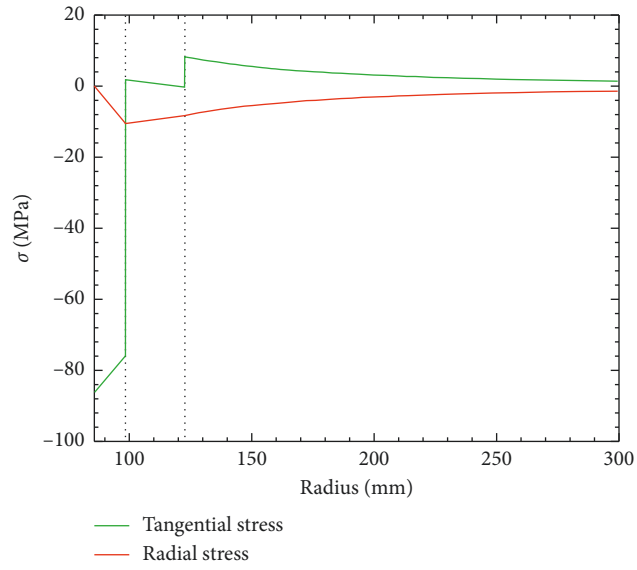

Figure 13: Stress variation of the system due to temperature change.

the maximum value at the inner surface of casing and changes to be tensile in the formation. For the cement sheath, the tangential stress is tensile at the inner surface and compressive at the outer surface.

Assume that in the production stage, the wellhead temperature increases from 20°C to 90°C, while the bottom hole (at 6300 m depth) temperature maintains 160°C. Temperature is assumed to distribute linearly with depth. Taking the cement inner surface as an example, the evolution of total stress with depth is shown in Figure 14. Comparing with the cement setting stage, radial compressive stress increases, and thus the ability of the system to resist microannulus increases. Tangential tensile stress increases, indicating the tensile failure risk of the cement sheath increases. Because temperature changes most at the wellhead, the radial and tangential stress variation is largest at the top of the well.

The evolution of the failure coefficient at the inner surface of cement sheath with depth is shown in Figure 15. Comparing Figure 15 and Figure 8, one can find that F value increases for constant volume or shrinking cement, while F decreases when the cement sheath expands in the cement setting stage.

The temperature rise in the production stage intensifies the risk of tensile failure and shear failure of cement sheath. Similar to the fracturing stage, the shrinkage of cement sheath has an adverse effect on the resistance to tensile failure, shear failure, and microannulus, while modest volume expansion of cement sheath is favorable to prevent these failure modes. In comparison with the fracturing stage, the stress variation caused by temperature difference within the cement sheath during the production stage is smaller than that caused by pressure difference in the fracturing stage. Therefore, the fracturing stage is a critical stage for the cement sheath integrity.

7. Conclusion

The evolution of stress inside the cement sheath is evaluated along the whole well life. Various conditions are considered including volume variation of the cement due to hydration during the cement setting stage, increase in casing pressure due to hydraulic fracturing during the completion stage, and casing heating during the production stage. The full-life-cycle analysis of the stress state inside the cement sheath serves to assess the potential failure modes (shear and tensile fracture and microannulus) of the cement sheath integrity, and the prevention measures can then be proposed.

Considering the loading history, two regimes should be distinguished. Before the solidification of cement, the cement is in liquid state and can merely withstand the hydraulic pressure, and thus the pressure in the casing and the in situ stress are supported by the casing and the rock, respectively. Only the stress increment occurring after solidification (such as fracture pressure) is withstood by the casing-cement-formation system.

The volume shrinkage of cement has an adverse effect on the resistance of the CSF system to tensile and shear failures and microannulus, whereas a modest volume expansion of the cement is favorable to the cement sheath integrity. Accordingly, the volume shrinkage of cement should be strictly controlled, and the cement slurry systems with no shrinkage or little expansion are recommended.

The cement sheath integrity is depth-dependent: in general, tensile failure, shear failure, and microannulus are more prone in the shallow layer. The pressure increase caused by hydraulic fracturing in the completion stage and the temperature rise in the production stage both lead to the decrease of the circumferential stress of the cement sheath, which adversely affects the integrity of the cement sheath. In particular, hydraulic fracturing is the most critical stage for the cement sheath integrity.

This article does not discuss the cement weightlessness at cement setting stage and the accumulated plastic of cement rings at staged fracturing process. These problems will be further studied in the future.

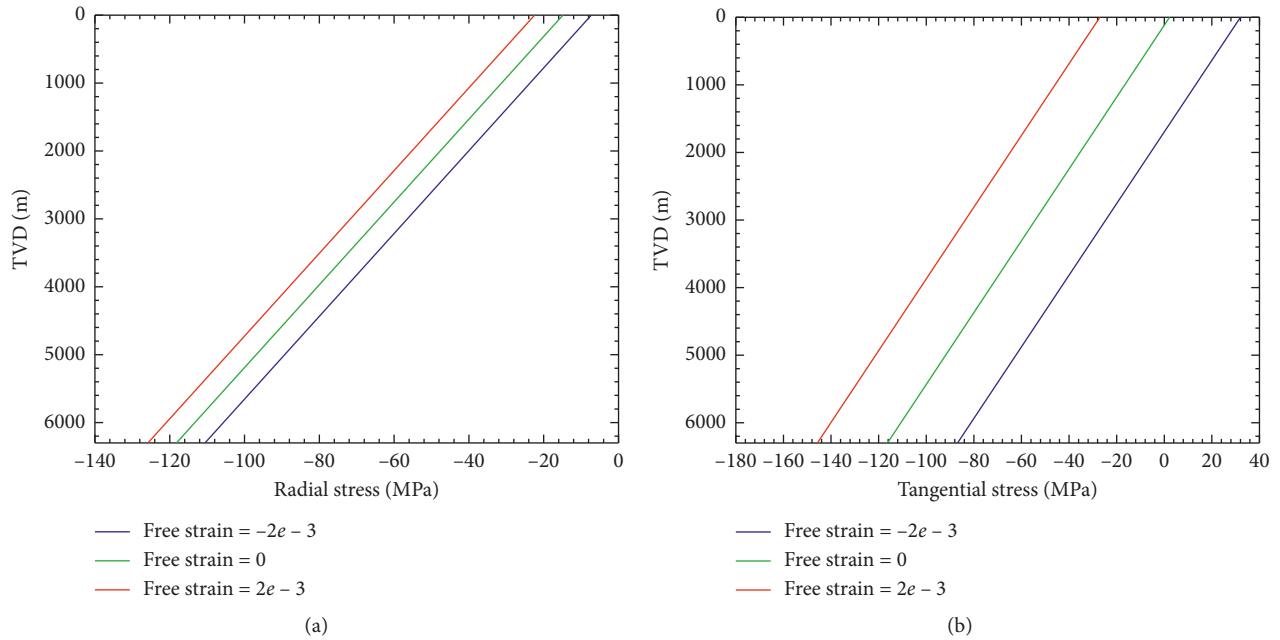

Figure 14: Evolution of the stress at the inner surface of cement sheath with depth in the production stage.

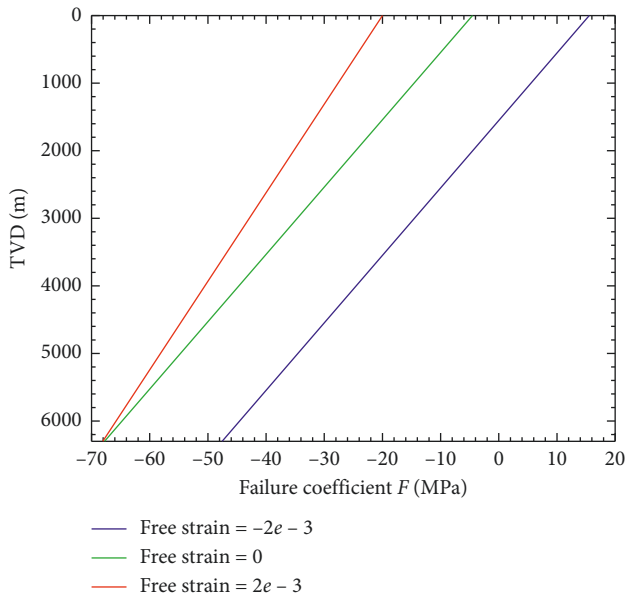

Figure 15: Failure coefficient at the inner surface of cement sheath at different depths in the production stage.

Symbols

r_1: Inner radius of casing (mm)
r_2: Outer radius of casing (mm)
r_3: Outer radius of cement sheath (mm)
P_c: Cement slurry pressure (MPa)
P_w: Fluid column pressure in casing (MPa)
P_0: Wellhead pressure in fracturing (MPa)
ρ_c: Cement slurry density (g/cm^3)
ρ_w: Fluid density in casing (g/cm^3)
ρ_f: Fracturing fluid density (g/cm^3)
g: Gravitational acceleration (m/s^2)
h: Vertical depth (m)
σ_H: Maximum horizontal principal compressive stress (MPa)
σ_h: Minimum horizontal principal compressive stress (MPa)
σ_{rr}: Radial stress (MPa)
$\sigma_{\theta\theta}$: Circumferential stress (MPa)
ε_{rr}: Radial strain
$\varepsilon_{\theta\theta}$: Circumferential strain
θ: The angle between the direction of maximum horizontal principal compressive stress σ_H (rad)
ε^c: Cement slurry free strain
ε^w: Casing free strain
ε^r: Rock free strain
u^i: Radial displacement of casing, cement sheath, and rock, m; the superscript i can be representatives for w (casing), c (cement), and r (rock), the same as in the following
E^i: Young's modulus of casing, cement sheath, and rock (GPa)
ν^i: Poisson's ratio of casing, cement sheath, and rock
X^i and Y^i: Unknown parameter
A: Calculation parameters used to determine the maximum and minimum principal stress
F: Mohr–Coulomb coefficient of determination (MPa)
φ: Internal friction angle of cement (rad)
C: Cement cohesion (MPa).

Data Availability

The data used to support the findings of this study are available from the corresponding author upon request.

Conflicts of Interest

The authors declare that they have no conflicts of interest.

Acknowledgments

This work was supported by the National Key Research and Development Program (grant no. 2016YFC0600901) and the open fund project of State Key Laboratory for Geomechanics & Deep Underground Engineering, China University of Mining & Technology (SKLGDUEK1718).

References

[1] B. Vignes and B. S. Aadnoy, "Well-integrity issues offshore Norway," in *Proceedings of the IADC/SPE Drilling Conference*, Society of Petroleum Engineers, Orlando, FL, USA, March 2008.

[2] W. Crow, J. W. Carey, S. Gasda, D. Brian Williams, and M. Celia, "Wellbore integrity analysis of a natural CO_2 producer," *International Journal of Greenhouse Gas Control*, vol. 4, no. 2, pp. 186–197, 2010.

[3] J. E. Johns, A. Frank, and D. Ross Mayfield, "Well integrity analysis in Gulf of Mexico wells using passive ultrasonic leak detection method," in *Proceedings of the SPE/ICoTA Coiled Tubing & Well Intervention Conference and Exhibition*, Society of Petroleum Engineers, The Woodlands, TX, USA, April 2011.

[4] C. Teodoriu, I. Obinna Ugwu, and J. J. Schubert, "Estimation of casing-cement-formation interaction using a new analythical model," in *Proceedings of the SPE EUROPEC/EAGE Annual Conference and Exhibition*, Society of Petroleum Engineers, Barcelona, Spain, June 2010.

[5] R. J. Davies, S. Almond, R. S. Ward et al., "Oil and gas wells and their integrity: implications for shale and unconventional resource exploitation," *Marine and Petroleum Geology*, vol. 56, pp. 239–254, 2014.

[6] R. B. Jackson, "The integrity of oil and gas wells," *Proceedings of the National Academy of Sciences*, vol. 111, no. 30, pp. 10902-10903, 2014.

[7] J. Kim, G. J. Moridis, and E. R. Martinez, "Investigation of possible wellbore cement failures during hydraulic fracturing operations," *Journal of Petroleum Science and Engineering*, vol. 139, pp. 254–263, 2016.

[8] M. B. Dusseault, M. S. Bruno, and B. John, "Casing shear: causes, cases, cures," in *Proceedings of the SPE International Oil and Gas Conference and Exhibition in China*, Society of Petroleum Engineers, Beijing, China, November 1998.

[9] A.-P. Bois, A. Garnier, F. Rodot, J. Sain-Marc, and N. Aimard, "How to prevent loss of zonal isolation through a comprehensive analysis of microannulus formation," *SPE Drilling & Completion*, vol. 26, no. 1, pp. 13–31, 2011.

[10] D. L. Newell and J. W. Carey, "Experimental evaluation of wellbore integrity along the cement-rock boundary," *Environmental Science & Technology*, vol. 47, no. 1, pp. 276–282, 2012.

[11] W. Chu, J. Shen, Y. Yang, Y. Li, and D. Gao, "Calculation of micro-annulus size in casing-cement sheath-formation system under continuous internal casing pressure change," *Petroleum Exploration and Development*, vol. 42, no. 3, pp. 414–421, 2015.

[12] Y. Q. Yin, Y. E. Cai, Z. W. Chen, and J. S. Liu, "Theoretical solution of casing loading in non-uniform ground stress field," *Acta Petrolei Sinica*, vol. 27, no. 4, pp. 133–138, 2006.

[13] H. Xu, N. Peng, T. Ma, and B. Yang, "Investigation of thermal stress of cement sheath for geothermal wells during fracturing," *Energies*, vol. 11, no. 10, p. 2581, 2018.

[14] H. Xu, T. Ma, N. Peng, and B. Yang, "Influences of fracturing fluid injection on mechanical integrity of cement sheath under four failure modes," *Energies*, vol. 11, no. 12, p. 3534, 2018.

[15] K. E. Gray, E. Podnos, and E. Becker, "Finite-element studies of near-wellbore region during cementing operations: part I," *SPE Drilling & Completion*, vol. 24, no. 1, pp. 127–136, 2009.

[16] H. Jo and K. E. Gray, "Mechanical behavior of concentric casing, cement, and formation using analytical and numerical methods," in *Proceedings of the 44th US Rock Mechanics Symposium and 5th US-Canada Rock Mechanics Symposium*, American Rock Mechanics Association, Salt Lake City, UT, USA, June 2010.

[17] P. Lura, O. M. Jensen, and K. Van Breugel, "Autogenous shrinkage in high-performance cement paste: an evaluation of basic mechanisms," *Cement and Concrete Research*, vol. 33, no. 2, pp. 223–232, 2003.

[18] F.-J. Ulm, G. Constantinides, and F. H. Heukamp, "Is concrete a poromechanics materials?-a multiscale investigation of poroelastic properties," *Materials and Structures*, vol. 37, no. 1, pp. 43–58, 2004.

[19] S. Ghabezloo, J. Sulem, S. Guédon, F. Martineau, and J. Saint-Marc, "Poromechanical behaviour of hardened cement paste under isotropic loading," *Cement and Concrete Research*, vol. 38, no. 12, pp. 1424–1437, 2008.

[20] O. Coussy, *Mechanics and Physics of Porous Solids*, John Wiley & Sons, Hoboken, NJ, USA, 2011.

[21] V. Baroghel-Bouny, "Water vapour sorption experiments on hardened cementitious materials: Part I: essential tool for analysis of hygral behaviour and its relation to pore structure," *Cement and Concrete Research*, vol. 37, no. 3, pp. 414–437, 2007.

[22] T. L. Anderson and T. L. Anderson, *Fracture Mechanics: Fundamentals and Applications*, CRC Press, Boca Raton, FL, USA, 2005.

[23] F.-J. Ulm and O. Coussy, "Strength growth as chemo-plastic hardening in early age concrete," *Journal of Engineering Mechanics*, vol. 122, no. 12, pp. 1123–1132, 1996.

[24] C. Teodoriu, C. Kosinowski, M. Amani, J. Schubert, and A. Shadravan, "Wellbore integrity and cement failure at HPHT conditions," *International Journal of Engineering*, vol. 2, no. 2, pp. 2305–8269, 2013.

[25] P. Wehling, "Wellbore cement integrity testing," Master's thesis, Technical University of Clausthal, Clausthal-Zellerfeld, Germany, 2008.